Yaw Rate and Sideslip Angle Control Through Single Input Single Output Direct Yaw Moment Control

Basilio Lenzo, *Member, IEEE*, Mattia Zanchetta, Aldo Sorniotti, *Member, IEEE*, Patrick Gruber, and Wouter De Nijs

Abstract—**Electric vehicles with independently controlled drivetrains allow torque vectoring, which enhances active safety and handling qualities. This article proposes an approach for the concurrent control of yaw rate and sideslip angle based on a single-input single-output (SISO) yaw rate controller. With the SISO formulation, the reference yaw rate is first defined according to the vehicle handling requirements and is then corrected based on the actual sideslip angle. The sideslip angle contribution guarantees a prompt corrective action in critical situations such as incipient vehicle oversteer during limit cornering in low tire-road friction conditions. A design methodology in the frequency domain is discussed, including stability analysis based on the theory of switched linear systems. The performance of the control structure is assessed via: 1) phase–plane plots obtained with a nonlinear vehicle model; 2) simulations with an experimentally validated model, including multiple feedback control structures; and 3) experimental tests on an electric vehicle demonstrator along step steer maneuvers with purposely induced and controlled vehicle drift. Results show that the SISO controller allows constraining the sideslip angle within the predetermined thresholds and yields tire-road friction adaptation with all the considered feedback controllers.**

Index Terms—**Controlled drift, electric vehicle, experimental tests, sideslip angle control, tire-road friction coefficient, torque vectoring (TV), yaw rate control.**

NOMENCLATURE

a	Front semiwheelbase.
a_x	Longitudinal acceleration.
a_y	Lateral acceleration.
A, B, C	State-space matrices of the plant.
A_i, B_i, C_i, D_i	State-space matrices of the plants considered in the stability analysis ($i = 1, 2, 3$).
A_s, B_s, C_s	State-space matrices of the shaped plant.

b	Rear semiwheelbase.
C_1	Front axle cornering stiffness.
C_2	Rear axle cornering stiffness.
d	Half-track width.
$D(s)$	Denominator of $G_{rM_Z}(s), G_{r\delta}(s), G_{\beta M_Z}(s)$, and $G_{\beta\delta}(s)$.
$D_H(s)$	Denominator of $G_{r\delta,H}(s)$ and $G_{\beta\delta,H}(s)$.
$D_S(s)$	Denominator of $G_{r\delta,S}(s)$ and $G_{\beta\delta,S}(s)$.
e_{int}	Integral of the yaw rate error.
f_i	Functions expressing the linearized vehicle dynamics model formulations.
F	Coefficient of the sideslip-based correction.
F_s	Matrix of the observer form implementation of the H_∞ controller.
F_X	Traction or braking force.
$G_{rM_Z}(s)$	Transfer function of yaw moment to yaw rate.
$G_{r\delta}(s)$	Transfer function of steering angle to yaw rate.
$G_{r\delta,H}(s)$	Transfer function of steering angle to yaw rate, handling case.
$G_{r\delta,S}(s)$	Transfer function of steering angle to yaw rate, stability case.
$G_{\beta M_Z}(s)$	Transfer function of yaw moment to sideslip angle.
$G_{\beta\delta}(s)$	Transfer function of steering angle to sideslip angle.
$G_{\beta\delta,H}(s)$	Transfer function of steering angle to sideslip angle, handling case.
$G_{\beta\delta,S}(s)$	Transfer function of steering angle to sideslip angle, stability case.
h_{max}	Maximum value of system uncertainties and disturbances.
H_s	Matrix of the observer form implementation of the H_∞ controller.
I	Identity matrix.
J_z	Yaw mass moment of inertia of the vehicle.
k	Ratio between r_h and δ in a simplified version of the yaw rate controller.
k_{a_y}	Factor for the definition of the reference yaw rate in the linearized model.
k_1, k_2	Tuning parameters of the sideslip-based correction.
K	Gain of the discontinuous part of the integral sliding mode controller (ISMC).
K_P	Proportional gain.
K_I	Integral gain.

m	Vehicle mass.
M_Z	Direct yaw moment.
$M_{Z,\text{ISMC}}$	Direct yaw moment from the ISMC.
$M_{Z,\text{PI}}$	Direct yaw moment from the proportional integral (PI) controller.
$M_{Z,\text{sw}}$	Discontinuous contribution of the ISMC.
$M_{Z,\text{sw},f}$	Filtered value of the discontinuous contribution of the ISMC.
N_*	Stability derivatives of the yaw moment balance equation of the single-track vehicle model, $* = \beta, r, \delta$.
$N_{rM_Z}(s)$	Numerator of $G_{rM_Z}(s)$.
$N_{r\delta}(s)$	Numerator of $G_{r\delta}(s)$.
$N_{\beta M_Z}(s)$	Numerator of $G_{\beta M_Z}(s)$.
$N_{\beta\delta}(s)$	Numerator of $G_{\beta\delta}(s)$.
$N_{r\delta,H}(s)$	Numerator of $G_{r\delta,H}(s)$.
$N_{\beta\delta,H}(s)$	Numerator of $G_{\beta\delta,H}(s)$.
$N_{r\delta,S}(s)$	Numerator of $G_{r\delta,S}(s)$.
$N_{\beta\delta,S}(s)$	Numerator of $G_{\beta\delta,S}(s)$.
p_w	Brake pressure demand for the w-th wheel ($w = 1, 2, 3, 4$).
p_a	Accelerator pedal position.
p_b	Brake pedal position.
P	Positive definite matrix.
r	Yaw rate.
r_h	Handling yaw rate.
r_{ref}	Reference yaw rate.
$r_{\text{ref,SS}}$	Steady-state reference yaw rate.
r_s	Stability yaw rate.
r_{sat}	Saturation yaw rate.
R_{wh}	Wheel radius.
s	Laplace operator.
t	Time.
t_{fin}	Final time of the relevant part of the maneuver.
t_{in}	Initial time of the relevant part of the maneuver.
u	Control input to the linearized model in the frequency domain study.
u_s	Control input to the shaped plant.
V	Vehicle speed.
Y_*	Stability derivatives of the lateral force equation of the single-track vehicle model, $* = \beta, r, \delta$.
$W(s)$	Transfer function of yaw rate error to direct yaw moment.
W_{PI}	Transfer function of the PI compensator.
W_s	Transfer function of the shaped plant.
x	State vector of the linearized model.
$\hat{x}_s$	Observer state vector of the shaped plant.
$\hat{y}_s$	Observer output vector of the shaped plant.
z	Term of the ISMC sliding variable.
Z_s, X_s	Solutions of the generalized algebraic Riccati equations of the H_∞ loop shaping optimization.
$\beta, \dot{\beta}$	Vehicle sideslip angle and sideslip rate at the center of mass.
β_{act}	Activation value of the sideslip-based correction.
β_D	Dynamic sideslip angle.

$\beta_{\text{ss,I}}, \beta_{\text{ss,II}}$	Steady-state values of β, i.e., the equilibria, in the phase–plane analyses.
β_{th}	Upper threshold of the sideslip-based correction.
δ	Steering angle at the wheel.
Δa_y	Tuning parameter of the sideslip-based correction.
ζ	Damping ratio associated with $D(s)$.
σ	Sliding variable.
σ_0	Conventional term of the sliding variable.
τ_w	Torque demand at the w-th wheel ($w = 1, 2, 3, 4$).
τ_{ISMC}	Time constant of the ISMC filter.
τ_L	Torque demand for the left side of the vehicle.
τ_R	Torque demand for the right side of the vehicle.
φ	Parameter of the solution of the algebraic Riccati equation.
ω_n	Natural frequency associated with $D(s)$.

I. INTRODUCTION

ELECTRIC vehicles with multiple motors allow torque vectoring (TV). This feature permits to generate a direct yaw moment through the controlled variation of the left-to-right wheel torque distribution. TV has been extensively studied in the literature as it enhances safety and drivability. For example, TV enables the design of the cornering response, i.e., to target a steady-state reference yaw rate characteristic, with the additional benefit of increasing yaw and sideslip damping during transients [1]–[9]. Moreover, TV systems can enhance energy efficiency [10]–[14].

Accurate estimation of the tire-road friction coefficient is required [15], [16] for the generation of the reference yaw rate. TV controllers using a reference yaw rate based on excessive values of the friction coefficient may lead to vehicle oversteer, i.e., a potentially dangerous vehicle response [17], [18], while a conservative estimate of the friction coefficient prevents the agility benefits of TV control. However, friction estimation [19]–[22] is difficult, especially for continuously active controllers, which require smooth profiles of the reference yaw rate. In fact, even a reasonably accurate estimation of the friction coefficient can generate drivability issues in TV systems, if it oscillates around the correct value. Such problem is less critical in production vehicles with stability controllers based on the actuation of the friction brakes, as they intervene only in emergency conditions. The tolerance on the yaw rate error before the system intervention compensates the effect of the reference yaw rate oscillations induced by the tire-road friction estimation. Moreover, it is much easier to estimate the friction coefficient from the measured longitudinal and lateral accelerations if the vehicle is already at the cornering limit, which is the case for stability controllers.

As an alternative to a reference yaw rate continuously dependent on the estimated tire-road friction conditions, the yaw rate controller of a TV system can be coupled with a sideslip angle controller. In fact, it is generally easier to estimate the vehicle sideslip angle than the tire-road friction coefficient [23].

The combined yaw rate and sideslip controllers are based on two inputs, i.e., a yaw rate and a sideslip angle related input, and produce a single value of direct yaw moment. However, as explained in [24], "it is not possible to control the yaw rate and the sideslip angle independently, using only the yaw moment. Trying to control both properties leads to a functionally uncontrollable system with uncontrollable directions. Controlling the lateral velocity (or the sideslip angle) and the yaw rate is possible only by including an additional device like an active steering system." Hence, if an additional actuation system is not available, the multivariable controller should include an appropriate algorithm to prioritize yaw rate or sideslip tracking depending on the driving conditions. The need for a careful design of the balance between the yaw rate and sideslip contributions is a challenging problem in terms of conventional linear control theory.

Several multivariable formulations for concurrent yaw rate and sideslip angle control have been proposed in the literature. For example, Esmailzadeh et al. [1] use a linear quadratic regulator where the direct yaw moment is a function of the yaw rate, the lateral component of the velocity of the center of gravity, and the steering angle, while the cost function minimizes the weighted combination of the yaw rate error and control effort, without considering vehicle sideslip. Although the lateral component of vehicle velocity is used in the formulation, the controller does not include any target sideslip angle value and is, thus, unable to stabilize the vehicle if the reference yaw rate is not compatible with the available tire-road friction conditions. De Novellis et al. [9] calculate two independent reference direct yaw moments, one based on the yaw rate error and the second one based on the sideslip deviation from a limit threshold. A separate empirical algorithm provides a variable weight between the yaw rate-based and sideslip-based yaw moment contributions, where the weighting depends on the current sideslip angle condition. In [25], the controller is based on a multivariable structure, receiving the yaw rate error and sideslip angle error as inputs, where the latter is set to zero for noncritical sideslip angles. However, the authors mention that a significant integral term in the yaw rate part of the controller provokes a progressive increase of the magnitude of the yaw rate-related reference yaw moment contribution, in the opposite direction with respect to the sideslip contribution. To this purpose, a correction of the reference yaw rate is proposed for the phases in which the sideslip angle contribution is active. Tchamna and Youn [26] use a first-order sliding mode formulation, where the sliding variable is a linear combination of the yaw rate error and sideslip angle, with a constant weight. The authors recommend a significant weight for the sideslip contribution; however, this would compromise vehicle responsiveness for a continuously active TV system. In [27], the feedforward yaw moment contribution targets a zero steady-state sideslip angle value, while the feedback contribution is based on an optimal controller with an objective function similar to that in [1]. The results show an important reduction of the steady-state yaw rate, i.e., of vehicle responsiveness, which would be unacceptable for the vehicle application of this article. Finally, the review

in [28] analyzes further references on the topic, reaching the conclusion that there is: 1) good theoretical work with no indication of the practical implications and 2) excellent practical work with little indication of control algorithms used.

A promising alternative method is represented by single-input single-output (SISO) yaw rate controllers, in which the reference yaw rate is corrected as a function of the actual sideslip angle. In this respect, Jalali et al. [29] modify the reference yaw rate with a contribution directly proportional to the estimated sideslip angle, which, however, does not allow setting up an actual soft constraint on vehicle sideslip, which is the requirement for effective stability control. Deur et al. [30] use a cascade control structure, where the reference lateral vehicle velocity is computed through a dynamic vehicle model. The lateral velocity error is sent to a proportional controller that outputs the reference yaw rate correction. The main limitations are the reliance on a linear reference vehicle model even when the vehicle is operating at the limits of handling, and the absence of a proposal for a control design procedure in the frequency domain, including stability assessment. The second limitation also applies to the method preliminarily proposed in [18]. Moreover, the mentioned references miss detailed analyses of the effect of the parameters of the sideslip contribution of the reference yaw rate on the system response, as these parameters are empirically tuned without considering the effect of the outer feedback loop using sideslip angle to modify the reference yaw rate.

In summary, the ideal reference yaw rate formulation should be able to indirectly constrain sideslip angle without relying on a dynamic vehicle model, and at the same time, it should be associated with a systematic methodology for stability demonstration, which is missing at the moment. This article covers this gap by further developing the formulation in [18], with the following novel contributions.

1) The methodology for the frequency response analysis and design, including verification of stability based on the theory of switched linear systems and consideration of the effect of the tuning parameters of the reference yaw rate formulation on the closed-loop vehicle response.

2) The validation of the reference yaw rate generation method via phase–plane analyses and vehicle dynamics simulations of scenarios with quickly variable tire-road friction coefficient, performed with a variety of control structures.

3) The experimental demonstration of the controller along a maneuver with purposely-induced vehicle drift, including sensitivity analyses of the main controller parameters.

This article is organized as follows. Section II presents the TV control structure and then focuses on the SISO formulation and its frequency domain analysis. Section III assesses the controller performance via: 1) phase–plane plots based on a simplified vehicle model with nonlinear tire characteristics and 2) vehicle dynamics simulations with an advanced vehicle model, using multiple approaches for the generation of the feedback yaw moment contribution. Finally, Section IV deals
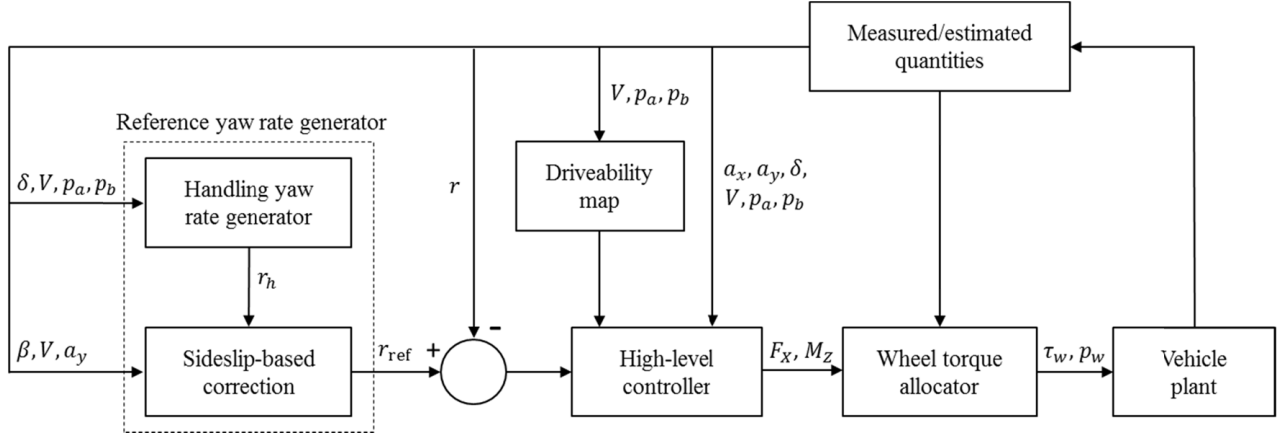
Fig. 1. Simplified schematic of the TV control structure.

with the experimental validation, leading to the summary in the conclusion section.

II. CONTROLLER DESIGN

A. Control Structure

Fig. 1 shows the simplified schematic of the TV control structure, which consists of the following blocks.

1) A reference yaw rate generator, including: a) a handling yaw rate generator, which defines the handling yaw rate, r_h, aimed at enhancing the steady-state cornering response in high tire-road friction conditions and b) a sideslip-based correction block, which corrects r_h based on the actual sideslip angle and defines the reference yaw rate, r_{ref}, as detailed in the remainder.

2) A high-level controller generating the traction/braking force demand, F_X, and the direct yaw moment demand, M_Z, starting from the outputs of a driveability map, the yaw rate error, and the measured or estimated states, e.g., vehicle accelerations, a_x and a_y, accelerator and brake pedal positions, p_a and p_b, vehicle speed, V, and steering angle, δ. As TV does not directly control the yaw moment contribution due to the lateral tire forces, M_Z is the yaw moment caused by the difference among the wheel torques on the left and right sides of the vehicle.

3) A wheel torque control allocator, which outputs the reference torques, τ_w, and brake pressures, p_w, for the individual wheels ($w = 1, 2, 3, 4$), corresponding to the desired values of F_X and M_Z generated by the high-level controller. Assuming that the front and rear vehicle track widths are the same, for small steering angles, the torque demands on the left and right sides of the vehicle, τ_L and τ_R, are expressed as follows:

$$\tau_L = 0.5 \left(F_X - \frac{M_Z}{d} \right) R_{wh}$$

$$\tau_R = 0.5 \left(F_X + \frac{M_Z}{d} \right) R_{wh}. \qquad (1)$$

In this work, within each side, the torque demand is equally distributed between the front and rear wheels.

Although several control allocation strategies are proposed in [13], [31], and [32], a simple control allocation is ideal for this study, as it focuses on the performance of the reference yaw rate generator and high-level controller.

B. Reference Yaw Rate Formulation

The proposed formulation is based on the idea that the absolute value of the vehicle sideslip angle, $|\beta|$, is relatively small during normal driving at reasonably high speed. Conversely, $|\beta|$ becomes considerable in critical conditions such as incipient oversteer. van Zanten [33] shows that the controllability of the vehicle cornering response through the steering system is maintained only if the vehicle is operating within a limited sideslip angle range.

To ensure this through a SISO control structure, in this study, the steady-state value of the reference yaw rate, $r_{\text{ref,SS}}$, is calculated as the weighted average of the handling yaw rate, r_h, and the stability yaw rate, r_s

$$r_{\text{ref,SS}} = r_h - F (r_h - r_s) \qquad (2)$$

where r_h represents the steady-state reference yaw rate for high tire-road friction conditions. In the on-line implementation of the controller, r_h is stored in look-up tables. These are generated through an optimization routine based on a nonlinear quasi-static vehicle model and a set of reference understeer characteristics [34], and define different driving modes, such as the normal mode, sport mode, and enhanced sport mode, each of them characterized by a different cornering response.

The weighting factor, F, depends on $|\beta|$

$$F = \begin{cases} 0, & \text{if } |\beta| < \beta_{\text{act}} \\ \dfrac{k_1(|\beta| - \beta_{\text{act}})}{\beta_{\text{th}} - \beta_{\text{act}}}, & \text{if } \beta_{\text{act}} \leq |\beta| \leq \beta_{\text{th}} \\ k_2, & \text{if } |\beta| > \beta_{\text{th}}. \end{cases} \qquad (3)$$

If $|\beta|$ is smaller than the activation threshold, β_{act}, the vehicle conditions are deemed safe, i.e., $F = 0$ and no correction is applied to r_h. If $|\beta|$ is larger than β_{act} but smaller than an upper threshold β_{th}, F linearly varies between 0 and $k_1 > 0$. If $|\beta|$ is larger than β_{th}, then $F = k_2 \geq k_1$, and $r_{\text{ref,SS}}$ is closer to

the stability yaw rate, r_s, which represents an achievable yaw rate in the current tire-road friction conditions

$$r_s = \begin{cases} r_h, & \text{if } |r_h| < |r_{\text{sat}}| \\ |r_{\text{sat}}|\text{sign}(r_h), & \text{if } |r_h| \geq |r_{\text{sat}}| \end{cases} \quad (4)$$

where r_{sat} is calculated from the measured lateral acceleration

$$r_{\text{sat}} = \frac{a_y - \text{sign}(a_y)\Delta a_y}{V}. \quad (5)$$

Equation (5) is a consequence of the fact that $r = a_y/V$ for small sideslip angles in steady-state cornering [35]. k_1, k_2, and $\Delta a_y \geq 0$ are tuning parameters, where Δa_y can be expressed as a function of the absolute value of lateral acceleration to provide some conservativeness to r_{sat}. Δa_y is the difference between the currently measured lateral acceleration, and the reference lateral acceleration used to bring the vehicle back to the desired sideslip angle level. Δa_y ensures that the sideslip angle is actually reduced when needed, and not only maintained (see also the sensitivity analyses in Section II-G). k_1 and k_2 determine the maximum influence of the sideslip contribution on the reference yaw rate. For example, if $k_1 = k_2 = 1$, in high sideslip conditions, the driver action in terms of steering wheel angle increase is substantially bypassed by the controller, which uses only the stability yaw rate (based on the saturation yaw rate) to calculate the reference yaw rate. If for the specific implementation, some dependency of the control action on the driver steering wheel input increase has to be maintained when the vehicle is in high sideslip conditions, values of k_1 and k_2 lower than 1 should be selected. Moreover, if $k_1 = k_2$, the transition from the second to the third condition of the sideslip-based variation of the reference yaw rate [see (3)] is smooth. On the contrary, by setting $k_2 > k_1$, it is possible to achieve a moderate intervention of the sideslip contribution for medium–high sideslip values and to have a more aggressive intervention once β_{th} is reached. The purpose of (2)–(5) is to indirectly constrain $|\beta|$ to remain within β_{th}. In this study, the sideslip angle is estimated or measured at the vehicle center of mass; however, alternative locations, e.g., the rear axle, can be used [18].

From $r_{\text{ref,SS}}$, the calculation of the reference yaw rate, r_{ref}, is carried out through a first order filter, which is tuned for each driving mode to provide the reference dynamics. The filter ensures that the transient reference response of the vehicle is reasonable. In fact, as the frequency response characteristic of any real vehicle subject to a steering wheel input has limited bandwidth, it would not be appropriate to set up a reference yaw rate based on a static formulation, which would not be achievable by the real plant for high-frequency inputs (see also [27]).

C. Model for Feedback Control System Design

Starting from the single-track vehicle model formulation [36], [37], under the hypotheses of small steering angles, linear tire behavior, and constant vehicle speed, the yaw rate can be expressed in the Laplace domain as follows:

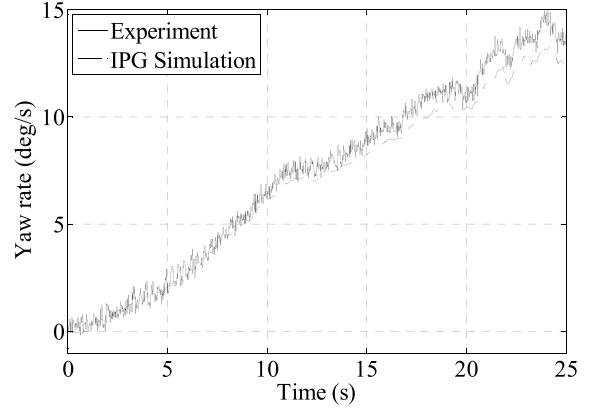$$r(s) = G_{rM_Z}(s)M_Z(s) + G_{r\delta}(s)\delta(s) \quad (6)$$

Fig. 2. Experimental validation of the CarMaker model during a skidpad test.

where the second-order transfer functions $G_{rM_Z}(s)$ and $G_{r\delta}(s)$ are given by

$$G_{rM_Z}(s) = \frac{N_{rM_Z}(s)}{D(s)} = \frac{mVs - Y_\beta}{J_z mVs^2 - (J_zY_\beta + N_r mV)s - N_\beta Y_r + N_\beta mV + N_r Y_\beta} \quad (7)$$

$$G_{r\delta}(s) = \frac{N_{r\delta}(s)}{D(s)} = \frac{N_\delta mVs + N_\beta Y_\delta - N_\delta Y_\beta}{J_z mVs^2 - (J_zY_\beta + N_r mV)s - N_\beta Y_r + N_\beta mV + N_r Y_\beta} \quad (8)$$

where $G_{rM_Z}(s)$ and $G_{r\delta}(s)$ depend on the vehicle stability derivatives [37], defined as follows:

$$Y_\beta = C_1 + C_2, \quad Y_r = \frac{aC_1 - bC_2}{V}, \quad Y_\delta = -C_1,$$

$$N_\beta = aC_1 - bC_2, \quad N_r = \frac{a^2 C_1 + b^2 C_2}{V}, \quad N_\delta = -aC_1. \quad (9)$$

Similarly, the sideslip angle response is given by

$$\beta(s) = G_{\beta M_Z}(s)M_Z(s) + G_{\beta\delta}(s)\delta(s) \quad (10)$$

where

$$G_{\beta M_Z}(s) = \frac{N_{\beta M_Z}(s)}{D(s)} = \frac{Y_r - mV}{D(s)}$$

$$G_{\beta\delta}(s) = \frac{N_{\beta\delta}(s)}{D(s)} = \frac{N_\delta Y_r - N_r Y_\delta - mVN_\delta + J_zY_\delta s}{D(s)}. \quad (11)$$

The values of the front and rear axle cornering stiffnesses, C_1 and C_2 in (9), were obtained via the following procedure.

1) Experimental skidpad tests (ISO 4138:2012) were performed with the electric vehicle demonstrator of the European project iCOMPOSE [38].
2) The measured steering wheel angle and vehicle speed profiles were input to an experimentally validated vehicle dynamics model in IPG CarMaker [39]. Fig. 2 shows the match between the simulation and experimental results during a test.
3) The time histories of the tire slip ratios, slip angles, camber angles, and vertical loads from the CarMaker

TABLE I
AXLE CORNERING STIFFNESS VALUES AT DIFFERENT
LATERAL ACCELERATIONS

Case no.	Lateral acceleration (m/s^2)	C_1 (N/rad)	C_2 (N/rad)
1	2.0	170200	175000
2	4.2	157500	166700
3	6.1	139000	152000
4	7.8	99000	125000
5	8.3	37180	82680
6	8.5	7212	79960

Fig. 4. Examples of the Bode plots of $(G_{rM_Z}(s)W_{PI}(s))/(1 + G_{rM_Z}(s) W_{PI}(s))$ for two speeds and cases of Table I.
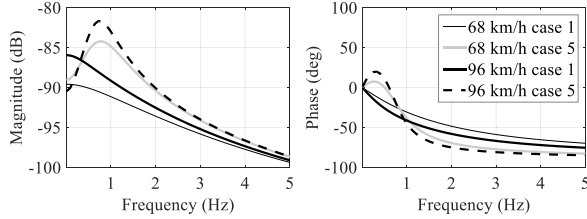

Fig. 3. Examples of the Bode plots of $G_{rM_Z}(s)$ for various speeds and cases of Table I.

model were input into the Pacejka magic formula [40] using the same parameterization as in the tire models of the CarMaker simulator.

4) C_1 and C_2 were obtained from the definition of axle cornering stiffness as incremental ratio of the total lateral force of the two tires on the same axle, with respect to the axle sideslip angle, by using the method in [41].

The resulting cornering stiffness values are reported in Table I, as functions of lateral acceleration, while Fig. 3 shows the significant variations of $G_{rM_Z}(s)$ with cornering stiffness and vehicle speed.

D. PI Controller Design

The reference yaw rate formulation of this study has implications on the cornering response of the vehicle with the TV controller. In the frequency domain, the reference direct yaw moment is given by

$$M_Z(s) = W(s)(r_{ref}(s) - r(s)) \qquad (12)$$

where $W(s)$ is the TV controller transfer function.

For example, Table II summarizes the design process of the PI TV controller, i.e., with $W(s) = W_{PI}(s) = K_P + K_I/s$. A gain scheduling scheme with vehicle speed is introduced for the proportional gain, K_P, to guarantee the same tracking bandwidth of the closed-loop system regardless of vehicle speed, which is typically a slowly-varying parameter. The bandwidth is here defined as the frequency value at which the magnitude of the response of the closed-loop system becomes 6 dB lower than its steady-state value. Table II reports: 1) the values of K_P; 2) the natural frequency, ω_n, and damping ratio, ζ, of $G_{rM_Z}(s)$; 3) the values of the gain and phase margins of the open-loop transfer function, $G_{rM_Z}(s)W_{PI}(s)$; and 4) the tracking bandwidth of the closed-loop transfer function, $G_{rM_Z}(s)W_{PI}(s)/(1 + G_{rM_Z}(s)W_{PI}(s))$, which is plotted for some cases in Fig. 4. The tuning of the TV controller is intentionally relatively relaxed in terms
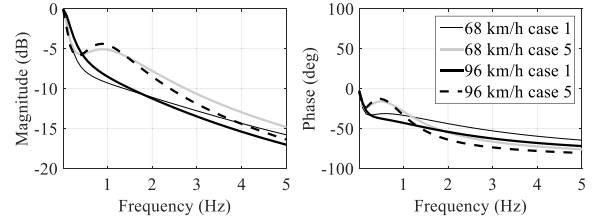
of tracking performance to ensure that the drivability of the vehicle is not compromised by the noise on the yaw rate sensor measurement, which can provoke undesired oscillations of the reference yaw moment.

The values of cornering stiffness for the tuning in Table II are those of case 5 in Table I. The stability properties of the feedback control system were verified for the other cases as well. The following paragraphs derive the response of the TV controlled vehicle to a steering wheel input for the two extreme cases in which: 1) the reference yaw rate coincides with the handling yaw rate and 2) the sideslip angle is larger than β_{th}, and thus, the reference yaw rate coincides with r_{sat}.

1) Handling Case (H) (Handling Yaw Rate as Reference): By imposing $r_{ref}(s) = r_h(s)$, assuming (for simplicity) that $r_h(s) = k\delta(s)$ in (12) and substituting back into (6), it is

$$r(s) = G_{r\delta,H}(s)\delta(s) = \frac{N_{r\delta,H}(s)}{D_H(s)}\delta(s) \qquad (13)$$

where the numerator and denominator of $G_{r\delta,H}(s)$ are

$$N_{r\delta,H}(s) = -mV(K_P + N_\delta)s^2$$
$$+ (K_P Y_\beta k - K_I mVk + N_\delta Y_\beta - N_\beta Y_\delta)s + K_I Y_\beta k$$
$$D_H(s) = -J_z mVs^3 + (J_z Y_\beta + mVN_r - K_P mV)s^2$$
$$+ (-N_r Y_\beta + K_P Y_\beta - K_I mV - mVN_\beta + N_\beta Y_r)s$$
$$+ K_I Y_\beta. \qquad (14)$$

Similarly, (10) becomes

$$\beta(s) = G_{\beta\delta,H}(s)\delta(s) = \frac{N_{\beta\delta,H}(s)}{D_H(s)}\delta(s) \qquad (15)$$

where the numerator of $G_{\beta\delta,H}(s)$ is

$$N_{\beta\delta,H}(s) = -J_z Y_\delta s^2 + ((mV - Y_r)(N_\delta + K_P k) + Y_\delta(N_r - K_P))s - K_I Y_\delta - K_I k(mV - Y_r). \qquad (16)$$

2) Stability Case (S) (Stability Yaw Rate as Reference): For large sideslip angles, i.e., for $|\beta| \geq \beta_{th}$, it is $r_{ref} = r_s = a_y/V$ when the steering input is large, $k_1 = k_2 = 1$ and $\Delta a_y = 0$. As from the vehicle kinematics, it is $a_y = V(r + \dot{\beta})$ [37], and thus, in the frequency domain $r(s) = a_y(s)/V - s\beta(s)$, (12) becomes for the case of the PI yaw rate controller

$$M_{Z,PI}(s) = W_{PI}(s)(r_{ref}(s) - r(s))$$
$$= sW_{PI}(s)\beta(s) = (K_I + sK_P)\beta(s) \qquad (17)$$

which is the formulation of a PI regulator on $\dot{\beta}$ or, equivalently, a proportional derivative (PD) regulator on β. This is consistent with the idea of controlling the sideslip angle rather than

TABLE II

MAIN TV SYSTEM PARAMETERS FOR DIFFERENT VEHICLE SPEEDS AND $K_I = 31623$ N · m/rad

Speed (km/h)	K_P (Nms/rad)	$G_{rM_Z}(s)$		$G_{rM_Z}(s)W_{\text{PI}}(s)$		$\dfrac{G_{rM_Z}(s)W_{\text{PI}}(s)}{1 + G_{rM_Z}(s)W_{\text{PI}}(s)}$
		ω_n (HZ)	ζ	Gain margin (dB)	Phase margin (deg)	Tracking bandwidth (Hz)
39	23806	0.986	0.665	Inf	144.9	1.434
56	18268	0.949	0.481	Inf	134.9	1.433
68	16058	0.937	0.401	Inf	127.4	1.433
79	14668	0.931	0.348	Inf	121.4	1.434
96	13152	0.925	0.288	Inf	114.0	1.432
102	12779	0.924	0.271	Inf	111.7	1.433

the yaw rate when the vehicle is in safety-critical conditions. As a note, with the adopted sign convention, for large sideslip angles (such as those targeted by the proposed sideslip-based correction), β has opposite sign from δ. By substituting (17) into (6), it is

$$r(s) = G_{r\delta,S}(s)\,\delta(s) = \frac{N_{r\delta,S}(s)}{D_S(s)}\delta(s) \qquad (18)$$

where $N_{r\delta,S}(s)$ and $D_S(s)$ are

$$N_{r\delta,S}(s) = -(mVN_\delta + K_P Y_\delta)s + N_\delta Y_\beta - Y_\delta(N_\beta + K_I)$$
$$D_S(s) = -mVJ_z s^2 + s(Y_\beta J_z + mVN_r - K_P(mV - Y_r))$$
$$+ (-Y_\beta N_r - (N_\beta + K_I)(mV - Y_r)). \qquad (19)$$

The sideslip response to a steering input is given by

$$\beta(s) = G_{\beta\delta,S}(s)\,\delta(s) = \frac{N_{\beta\delta,S}(s)}{D_S(s)}\delta(s) \qquad (20)$$

with $N_{\beta\delta,S}(s)$ being

$$N_{\beta\delta,S}(s) = -J_z Y_\delta s + N_r Y_\delta + N_\delta(mV - Y_r). \qquad (21)$$

The static gain of $G_{\beta\delta,S}$ given by

$$G_{\beta\delta,S}(s=0) = \frac{N_r Y_\delta + N_\delta(mV - Y_r)}{-Y_\beta N_r - (N_\beta + K_I)(mV - Y_r)} \qquad (22)$$

does not depend on K_P, decreases with increasing values of K_I, and tends to 0 for $K_I \to \infty$.

E. Linearized Models of the Controlled System

To evaluate the frequency response of the vehicle with the TV controller, the controlled plant is reduced to a formulation where the steering angle is the only input, and the expression of the reference direct yaw moment is substituted into the dynamic equations of the vehicle model.

Because of the PI formulation of the considered feedback controller, a third system state is introduced, i.e., the integral of the yaw rate error

$$e_{\text{int}} = \int (r_{\text{ref}} - r)\,dt. \qquad (23)$$

After substituting (23) into (6)–(11), the model equations become

$$\dot{\beta} = -\frac{Y_\beta}{Vm}\beta + \left(\frac{Y_r}{Vm} - 1\right)r + \frac{Y_\delta}{Vm}\delta \qquad (24)$$

$$\dot{r} = -\frac{N_\beta}{J_z}\beta - \frac{N_r}{J_z}r - \frac{N_\delta}{J_z}\delta + \frac{1}{J_z}(K_P(r_{\text{ref}} - r) + K_I e_{\text{int}}) \qquad (25)$$

$$\dot{e}_{\text{int}} = r_{\text{ref}} - r. \qquad (26)$$

Moreover, in the reference yaw rate formulation of (2), it is imposed that: 1) $|r_h| \geq |r_{\text{sat}}|$ in the calculation of r_s, as this condition is usually met during cornering at the limit of handling and 2) $\text{sign}(a_y)\Delta a_y \approx k_{a_y}a_y = k_{a_y}V(r + \dot{\beta})$, as the magnitude of this term of r_{sat} can be tuned as an increasing function of the absolute value of lateral acceleration, and its sign varies with a_y. Hence, the rearranged (2) becomes

$$r_{\text{ref}} = k\delta - F(k\delta - (1 - k_{a_y})(r + \dot{\beta})) \qquad (27)$$

where F is given by (3), which defines three cases, depending on $|\beta|$.

For each case, the result is a system of three equations, which can be expressed as follows:

$$\dot{x}(t) = f_i(x, u, t) \qquad (28)$$

where $x = [\beta, r, e_{\text{int}}]^{\text{T}}$ is the state vector, and the subscript i indicates the case. Two of the system formulations, i.e., those for $F = 0$ and $F = k_2$, are linear, with system matrices that are invariant with respect to the linearization point, while the third formulation, i.e., the one for $0 < F < k_2$, is nonlinear, and in this study, it is linearized around a specified condition.

To account for the discontinuity in the formulation of F caused by the absolute value of the sideslip angle, during the linearization, in the computation of the partial derivatives, $|\beta|$ is replaced by $\sqrt{\beta^2}$, thus obtaining

$$\frac{d|\beta|}{dr}\bigg|_{\substack{r=r_0 \\ \beta=\beta_0 \\ e_{\text{int}}=e_{\text{int},0} \\ \delta=\delta_0}} = \frac{d|\beta|}{de_{\text{int}}}\bigg|_{\substack{r=r_0 \\ \beta=\beta_0 \\ e_{\text{int}}=e_{\text{int},0} \\ \delta=\delta_0}} = 0, \quad \frac{d|\beta|}{d\beta}\bigg|_{\substack{r=r_0 \\ \beta=\beta_0 \\ e_{\text{int}}=e_{\text{int},0} \\ \delta=\delta_0}} = \frac{\beta_0}{|\beta_0|} \qquad (29)$$

where the linearization point is indicated by the subscript "0." The state-space matrices were computed with the symbolic

TABLE III
MAIN PARAMETERS OF THE LINEARIZED MODELS

Parameter	Value	Unit
V	26.67	m/s
r_0	0.33	rad/s
β_0	-0.13	rad
$e_{int,0}$	0.08	rad
δ_0	0.13	rad
k	2.7	s^{-1}
β_{act}	0.10	rad
β_{th}	0.26	rad
k_{a_y}	0.112	-
k_1	1	-
k_2	1	-

Fig. 5. Bode plots of the magnitude of r/δ and β/δ for the passive vehicle, the controlled vehicle with $F = 0$ (handling case), the controlled vehicle with $F = 1$ (stability case), and the controlled vehicle with $0 < F < 1$.

calculation software Maple [42]

$$A_i = \begin{bmatrix} \dfrac{\partial f_1}{\partial r} & \dfrac{\partial f_1}{\partial \beta} & \dfrac{\partial f_1}{\partial e_{int}} \\ \dfrac{\partial f_2}{\partial r} & \dfrac{\partial f_2}{\partial \beta} & \dfrac{\partial f_2}{\partial e_{int}} \\ \dfrac{\partial f_3}{\partial r} & \dfrac{\partial f_3}{\partial \beta} & \dfrac{\partial f_3}{\partial e_{int}} \end{bmatrix}_{\substack{r=r_0 \\ \beta=\beta_0 \\ e_{int}=e_{int,0} \\ \delta=\delta_0}}, \quad i = 1, 2, 3$$

$$B_i = \begin{bmatrix} \dfrac{\partial f_1}{\partial \delta} \\ \dfrac{\partial f_2}{\partial \delta} \\ \dfrac{\partial f_3}{\partial \delta} \end{bmatrix}_{\substack{r=r_0 \\ \beta=\beta_0 \\ e_{int}=e_{int,0} \\ \delta=\delta_0}}, \quad C_i = I_{3 \times 3}, \quad D_i = 0_{3 \times 1}. \quad (30)$$

For $0 < F < 1$, the linearization point was selected by imposing a yaw rate and a vehicle speed, and by reversing the model equations in steady-state conditions to obtain the corresponding sideslip angle, integral of the yaw rate error, and steering angle. Table III indicates the main parameters used in the following stability and frequency response analyses.

F. Stability Analysis of the Resulting Switched Linear System

The linearized vehicle model of Section II-E has three formulations, depending on the value of β. Hence, the model has the typical configuration of a switched linear system [43], and its stability cannot be inferred only by ensuring that the poles of the transfer functions for each individual case have a negative real part, as the system must also be stable when there is no restriction on the switching signal.

According to [43], if the existence of a common quadratic Lyapunov function for all three formulations of the vehicle model can be proven, then the system is quadratically stable, which guarantees that it is also asymptotically stable. A sufficient stability condition can be formalized through the following set of linear matrix inequalities (LMIs):

$$PA_i + A_i^T P < 0, \quad i = 1, 2, 3, \quad P \in \mathbb{R}^{3 \times 3}, \text{ symmetric.} \quad (31)$$

Hence, ensuring system stability translates into finding a symmetric positive definite matrix P with the same size as A_i, which meets the inequalities in (31).
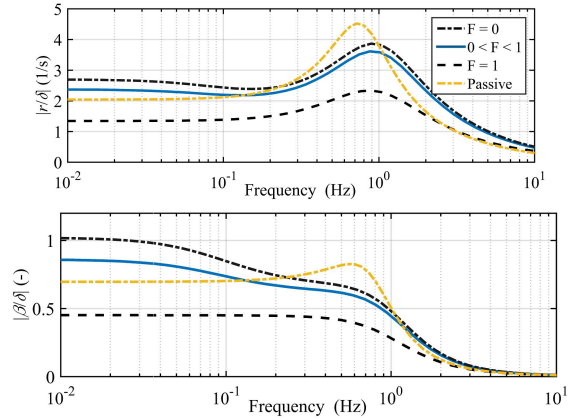
The problem in (31) was solved by using the optimization toolbox Yalmip [44] and the semidefinite programming solver SeDuMi [45], which were interfaced with the state-space formulations in MATLAB. The inequalities were imposed as constraints of the optimization, and the decision variables were the entries of P. For example, for the parameters in Table III, the optimizer returns the following P matrix:

$$P = \begin{bmatrix} 0.9377 & 0.0614 & -0.1645 \\ 0.0614 & 0.0656 & -0.0389 \\ -0.1645 & -0.0389 & 0.7072 \end{bmatrix}. \quad (32)$$

With this choice of P, the inequalities in (31) are satisfied and the system is asymptotically stable. The optimization was also run for all the cases covered in the sensitivity analyses of Section II-G, and the optimizer always returned a valid solution for the LMIs.

G. Effect of the Tuning Parameters of the Reference Yaw Rate

The transfer functions corresponding to the state-space systems in (30) are used for the analysis of the system frequency response. For example, Fig. 5 reports the Bode plots of the magnitude of r/δ and β/δ of the passive vehicle and the three TV controlled cases. The controlled vehicle exhibits reduced resonance peaks and larger bandwidth than the passive one. In the Bode plots, the static gains for $F = 0$, i.e, when the reference yaw rate depends only on the handling yaw rate, are greater than those of the passive vehicle, which is typical of the sport driving mode [34], designed to reduce understeer. The static gains for $F = 1$ (note that $k_1 = k_2 = 1$ in Table III), i.e., when the reference yaw rate is based only on the stability yaw rate, are lower than for the passive vehicle, and the sideslip angle is reduced over the whole frequency range. As expected, for $0 < F < 1$, the response is between that for the handling and stability cases.

The system behavior is influenced by the selected values of thresholds and tuning parameters. For example, Fig. 6 shows a sensitivity analysis on $\Delta a_{y,0} \approx k_{a_y} a_{y,0} = k_{a_y} V r_0$, which is varied between 0 and 4.5 m/s^2, through a corresponding variation of k_{a_y}. Interestingly, $\Delta a_{y,0}$ primarily affects the
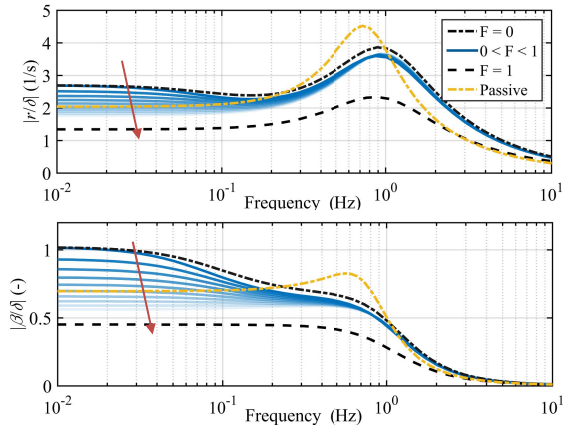
Fig. 6.   Bode plots of the magnitude of r/δ and β/δ for the passive vehicle, the controlled vehicle with $F = 0$ (handling case), the controlled vehicle with $F = 1$ (stability case), and the controlled vehicle with $0 < F < 1$, for increasing values of $\Delta a_{y,0}$, as indicated by the direction of the arrows.
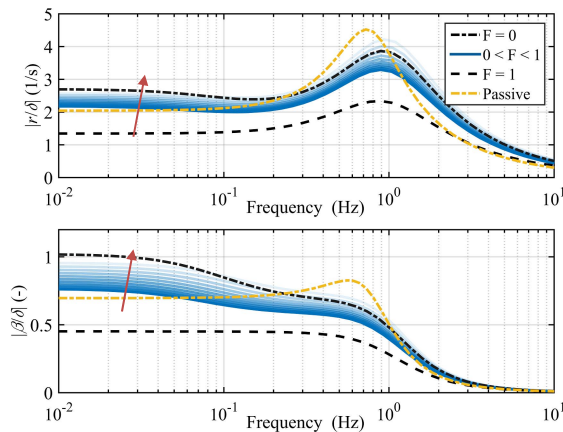

Fig. 7.   Bode plots of the magnitude of r/δ and β/δ for the passive vehicle, the controlled vehicle with $F = 0$ (handling case), the controlled vehicle with $F = 1$ (stability case), and the controlled vehicle with $0 < F < 1$, for increasing values of β_{act}, as indicated by the direction of the arrows.

steady-state gain, which decreases with increasing $\Delta a_{y,0}$, as indicated by the direction of the arrows. In particular, setting $\Delta a_{y,0} = 0$ causes the steady-state gain to be the same as for the controlled vehicle using the handling yaw rate.

Fig. 7 reports the sensitivity analysis on the value of the lower activation threshold, β_{act}, which is progressively increased from 0 to 9° and affects the response along the whole frequency range. As expected from (3), the increase of β_{act} brings the linearization point closer to the handling case, which explains the trend of the frequency response to approach that for $F = 0$. Similar trends were obtained in the sensitivity analysis on β_{th}. A high value of the threshold reduces F [see (3)], which makes the reference yaw rate closer to that of the handling case.

H. Assessed Control Structures

The reference yaw rate formulation of Section II-B has general validity, i.e., it can be coupled with any SISO control structure. The following controllers will be used and compared in Sections III and IV.

1) A yaw rate controller without the sideslip-based correction of the reference yaw rate, using the PI design of Section II-D, coupled with the integral sliding mode contribution of [46] and [47], implemented as a perturbation compensator providing robustness against matched disturbances. This formulation will be indicated as YR-ISMC in the remainder. The direct yaw moment control action, $M_{Z,\mathrm{ISMC}}$, is given by the sum of the PI yaw moment contribution, $M_{Z,\mathrm{PI}}$, and the filtered value, $M_{Z,\mathrm{sw},f}$, of the discontinuous term, $M_{Z,\mathrm{sw}}$, providing robustness against matched disturbances

$$M_{Z,\mathrm{ISMC}} \cong M_{Z,\mathrm{PI}} + M_{Z,\mathrm{sw},f}. \tag{33}$$

$M_{Z,\mathrm{sw},f}$ is calculated as follows:

$$\dot{M}_{Z,\mathrm{sw},f}\,\tau_{\mathrm{ISMC}} + M_{Z,\mathrm{sw},f} = M_{Z,\mathrm{sw}} \tag{34}$$

where $M_{Z,\mathrm{sw}}$ is obtained from

$$M_{Z,\mathrm{sw}} = -J_z K \,\mathrm{sign}(\sigma), \quad \text{with } K > |h_{\max}|. \tag{35}$$

The inequality expresses the Lyapunov stability condition based on the magnitude of the system disturbances and uncertainties (see [46] for its derivation). The sliding variable is the sum of the yaw rate error, $r - r_{\mathrm{ref}}$, which is equal to the conventional part of the sliding variable, σ_0, typical of any sliding mode formulation, and the auxiliary term, z, which is exclusive of ISMC:

$$\sigma = r - r_{\mathrm{ref}} + z = \sigma_0 + z. \tag{36}$$

In the specific implementation, z is calculated as the integral of $\dot{z}$ (the theory is detailed in [48])

$$\dot{z} = -\frac{d\sigma_0}{d(r - r_{\mathrm{ref}})}\left[-\dot{r}_{\mathrm{ref}} + \frac{1}{J_z}(M_{Z,\mathrm{ISMC}} - M_{Z,\mathrm{sw}})\right]$$
$$= \dot{r}_{\mathrm{ref}} - \frac{1}{J_z}(M_{Z,\mathrm{ISMC}} - M_{Z,\mathrm{sw}}). \tag{37}$$

2) The same controller as in 1), but with the reference yaw rate based on the formulation in Section II-B. This controller will be indicated as ISMC.

3) An H_∞ formulation based on loop shaping (see [41], [49], [50] for the details) indicated as H_∞ in the remainder, including the reference yaw rate correction of Section II-B. The controller is based on the conversion of the transfer function G_{rM_Z} into a state-space form, parameterized with V

$$G_{rM_Z}(V) = \begin{bmatrix} A(V) & B(V) \\ C(V) & 0 \end{bmatrix}. \tag{38}$$

$G_{rM_Z}(V)$ is multiplied by the precompensator W_{PI}, with proportional and integral gains equal to those of the PI controller in 1) and 2). For the H_∞ gain scheduling scheme, four speed values were selected. The transfer function of the shaped plant is

$$W_s(V) = W_{\mathrm{PI}}(V)G_{rM_Z}(V) = \begin{bmatrix} A_s(V) & B_s(V) \\ C_s(V) & 0 \end{bmatrix}. \tag{39}$$
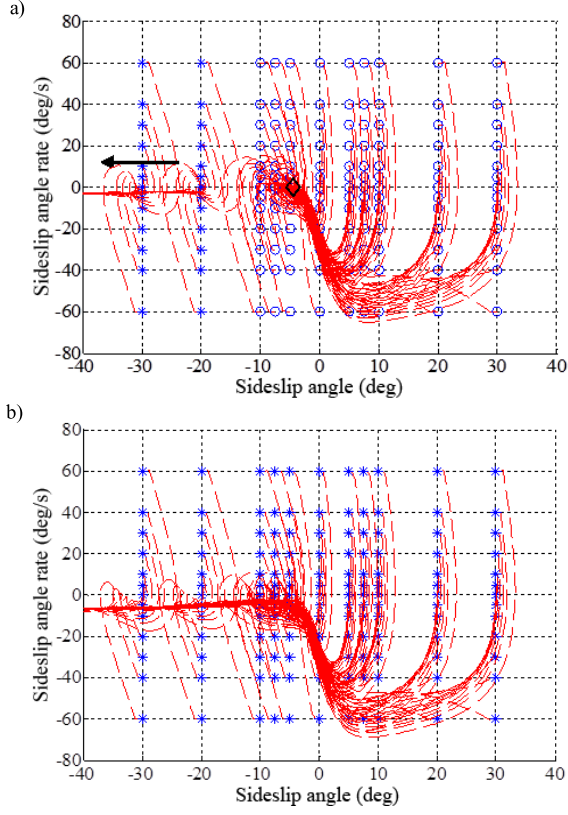
a)

b)

Fig. 8. Phase–plane plots for the vehicle with the YR-ISMC, 80 km/h, 50° of steering wheel angle. (a) Sport mode. (b) Enhanced sport mode. ∗: Unstable initial conditions; ◯: Stable initial conditions; and ◇: Equilibrium ($\beta_{ss,I}$).

a)

b)

Fig. 9. Phase–plane plots for the vehicle with the ISMC ($\beta_{act} = 13°$, $\beta_{th} = 14°$, and $\Delta a_y = 0$ m/s²), 80 km/h, and 50° of steering wheel angle. (a) Sport mode. (b) Enhanced sport mode. ◯: Stable initial conditions that converge to ◇; ×: Stable initial conditions that converge to □; ◇: Equilibrium ($\beta_{ss,I}$) of the vehicle with the YR-ISMC; and □: Second equilibrium ($\beta_{ss,II}$) of the vehicle with the ISMC.

The H_∞ loop shaping controller is implemented in the observer/state feedback form

$$\begin{cases} \dfrac{d\hat{x}_s}{dt} = A_s(V)\hat{x}_s + H_s(V) \\ \qquad \times (C_s(V)\hat{x}_s - \hat{y}_s) + B_s(V)u_s \\ u_s = F_s\hat{x}_s \end{cases} \tag{40}$$

where

$$\begin{cases} H_s(V) = -Z_s^{\mathrm{T}}(V)C_s^{\mathrm{T}}(V) \\ F_s(V) = -B_s^{\mathrm{T}}(V)(I - \varphi^{-2}I - \varphi^{-2}X_s)^{-1}X_s. \end{cases} \tag{41}$$

Z_s and X_s are the solutions of the generalized algebraic Riccati equations of the H_∞ loop shaping optimization [49]. The gain scheduling scheme on V was implemented according to the stability preserving interpolation method in [51].

4) A controller with the same PI as in controllers (1)–(3), including the sideslip-based reference yaw rate modification, and coupled with a static nonlinear feedforward contribution. The feedforward contribution is designed according to [34], and corrected through the factor $r_{\mathrm{ref,SS}}/r_h$, which provides an estimation of the actual tire-road friction coefficient at the limits of handling. Such configuration will be indicated as FF + PI.
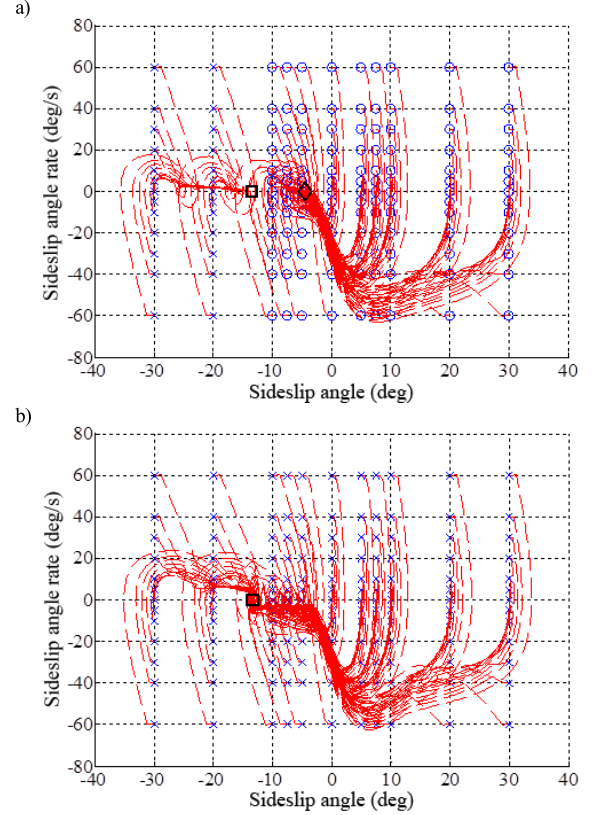
III. SIMULATION RESULTS

A. Phase–Plane Analysis

The phase–plane analysis uses a simplified nonlinear double-track vehicle model, which takes into account the lateral load transfers in the computation of the lateral tire forces through the magic formula for pure cornering. The simulator includes the YR-ISMC and ISMC TV formulations. The TV yaw moment is directly applied as an input to the yaw moment balance equation. Several combinations of β and $\dot{\beta}$ are imposed as initial conditions for the model, which is run for a high tire-road friction coefficient with constant steering wheel angle (50°) and vehicle speed (80 km/h) [25], [52]. This process identifies the set of initial conditions providing stable response.

Fig. 8(a) shows that with the YR-ISMC and sport mode, the vehicle converges to the equilibrium $\beta_{ss,I} = -4.5°$ as long as the initial conditions imply $\beta \geq -10°$; for all other initial conditions, the system response diverges. Fig. 8(b) refers to the enhanced sport mode, which is characterized by large values of $|r_h|$, i.e., beyond the cornering limit for the assigned steering wheel angle, to purposely induce vehicle drift. As expected, in this driving mode, all points diverge with the YR-ISMC.

The benefit of the sideslip-based correction of the reference yaw rate is evident in Fig. 9, where the system converges regardless of the initial conditions. In particular, in the sport
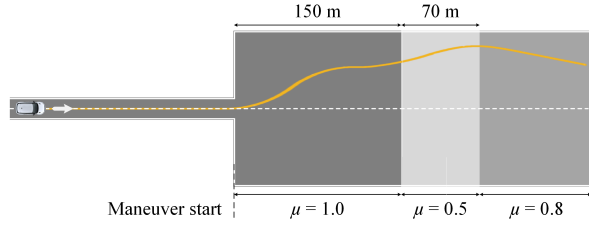
Fig. 10.   Top view of the simulation scenario. The colors indicate different values of the tire-road friction coefficient, μ. The continuous line is an example of vehicle trajectory during the maneuver.

mode [see Fig. 9(a)], two equilibria exist. In fact, the same points as in the YR-ISMC case converge to the equilibrium of $\beta_{ss,I} = -4.5°$ Fig. 8(a). In addition, the points that were unstable become stable and converge to a second equilibrium, $\beta_{ss,II} = -13.4°$. $\beta_{ss,II}$ mainly depends on β_{act} and β_{th}, and the difference $\beta_{th} - \beta_{act}$. In the enhanced sport mode [see Fig. 9(b)], all points converge to $\beta_{ss,II}$, which demonstrates the effectiveness of the induced vehicle drift control of such driving mode.

B. CarMaker Simulations

The CarMaker model of Section II-C is used for the validation of the reference yaw rate formulation with the controllers of Section II-H in a very challenging scenario (Fig. 10). The simulated maneuver is a multiple step steer test, i.e., a sequence of fast steering wheel angle variations applied at a rate of $\pm 400°/s$, followed by constant steering wheel angle phases, each of them 2 s long. The steering angle values after the steering applications are $100°$, $-100°$, $120°$, $-120°$, and $0°$ [see Fig. 11(a)]. The tests are executed in the sport mode with a constant total wheel torque demand and an initial speed of 90 km/h. To evaluate the adaptability of the proposed reference yaw rate scheme, the scenario includes tire-road friction coefficient discontinuities (Fig. 10), i.e., the friction coefficient is 1 at the beginning of the maneuver, reduced to 0.5 after 150 m (at ≈ 6.5 s), and increased to 0.8 after further 70 m (at ≈ 9.8 s).

The following performance indicators are defined to objectively evaluate the controllers.

1) The RMSE_r, which assesses the yaw rate tracking performance

$$\text{RMSE}_r = \sqrt{\frac{1}{t_{fin} - t_{in}} \int_{t_{in}}^{t_{fin}} (r_{ref}(t) - r(t))^2 dt}. \quad (42)$$

2) The RMSE_β, which assesses the significance of the sideslip-based correction of the reference yaw rate

$$\text{RMSE}_\beta = \sqrt{\frac{1}{t_{fin} - t_{in}} \int_{t_{in}}^{t_{fin}} (r_{ref,SS}(t) - r_h(t))^2 dt}. \quad (43)$$

3) The IACA, which assesses the significance of the direct yaw moment control action

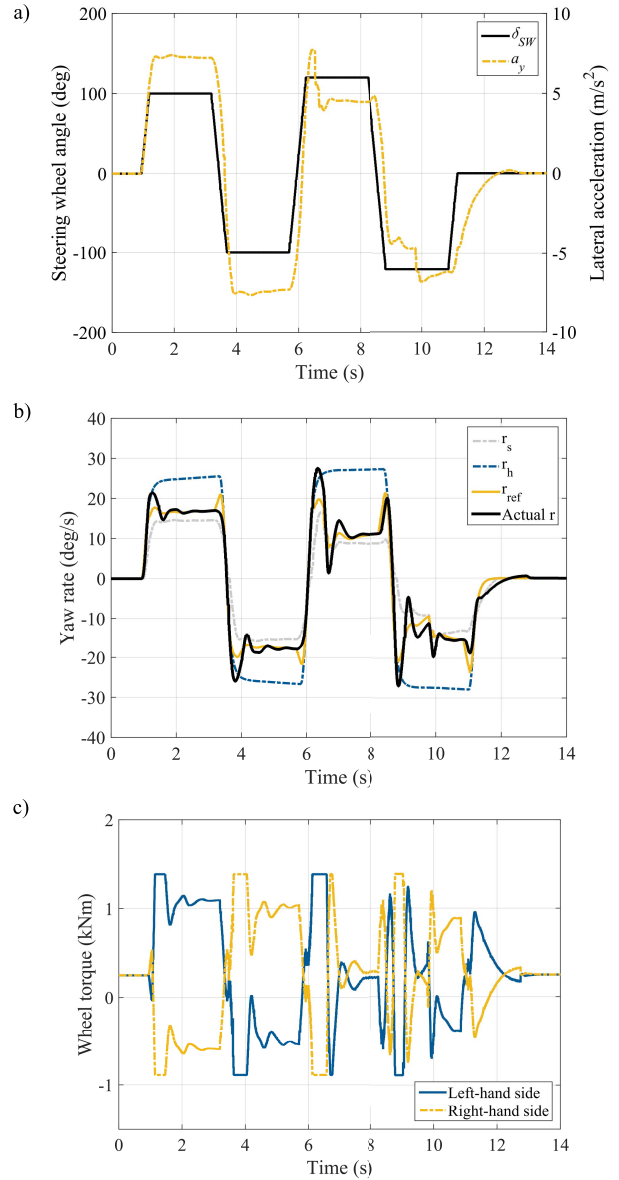$$\text{IACA} = \frac{1}{t_{fin} - t_{in}} \int_{t_{in}}^{t_{fin}} |M_Z(t)| dt. \quad (44)$$

Fig. 11.   Simulation results, sport mode, multiple step steers, variable tire-road friction conditions, 90 km/h, ISMC ($\Delta a_y = 1$ m/s^2, $k_1 = k_2 = 1$, $\beta_{act} = 1.5°$, and $\beta_{th} = 6°$). (a) Steering wheel angle and lateral acceleration. (b) Yaw rates. (c) Total left- and right-hand sides wheel torque levels.

t_{in} and t_{fin} represent the time at the beginning of the maneuver, and the time at the completion of the maneuver, i.e., 3 s after the steering wheel input is back to 0.

Fig. 11 shows the response for the ISMC formulation, which is compared with that of the passive vehicle and the vehicle with the YR-ISMC in Fig. 12. Table IV reports the performance indicators for the controllers of Section II-H, and the peak values of $|\beta|$ and $|\beta_D|$, where β_D is the dynamic sideslip angle, i.e., the difference between the actual sideslip angle and the sideslip angle in kinematic steering conditions.

The ISMC maintains the sideslip angle within the defined threshold (see Fig. 12(a) and Table IV), regardless of the tire-road friction coefficient, guaranteeing an intrinsic tire-road

TABLE IV
PERFORMANCE INDICATORS FOR THE SIMULATED MULTIPLE STEP STEER TESTS ($\Delta a_y = 1$ m/s^2 AND $k_1 = k_2 = 1$ FOR THE FF + PI, H$_\infty$, AND ISMC)

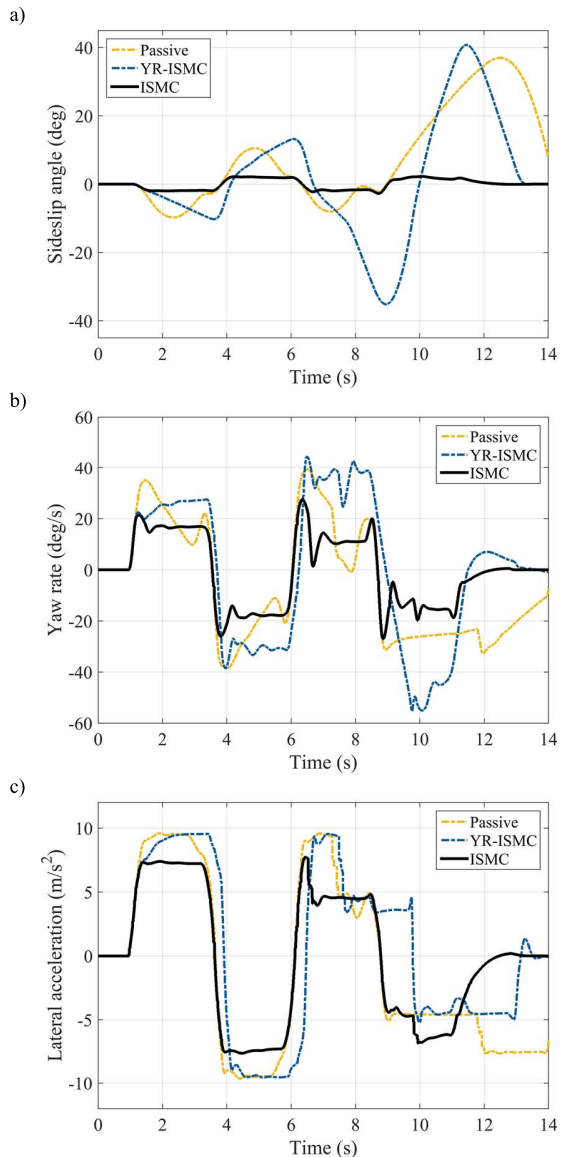|	Passive	YR-ISMC	FF+PI	H$_\infty$	ISMC
RMSE$_r$ (deg/s)	13.75	16.77	4.34	4.17	2.52
RMSE$_\beta$ (deg/s)	NA	0	9.81	9.41	9.50
IACA (Nm)	NA	2097	1161	2193	2162
max$|\beta|$ (deg)	36.98	40.76	4.76	3.05	2.72
max$|\beta_D|$ (deg)	36.98	40.76	7.91	6.83	6.06

a)

b)

c)

Fig. 12. Simulation results, sport mode, multiple step steers, variable tire-road friction conditions, 90 km/h, for: 1) Passive vehicle; 2) YR-ISMC; and 3) ISMC ($\Delta a_y = 1$ m/s^2, $k_1 = k_2 = 1$, $\beta_{act} = 1.5°$, and $\beta_{th} = 6°$). (a) Sideslip angle. (b) Yaw rate. (c) Lateral acceleration.

friction adaptation with a simple control structure. Instead, the YR-ISMC exhibits sideslip angle peaks even larger than those of the passive vehicle, because of the "aggressive" cornering characteristics (i.e., less understeering) of the sport mode, and the lack of the sideslip-based adaptation of the reference yaw rate to the tire-road friction level.

A detailed analysis of the ISMC behavior in Figs. 11 and 12 shows the following.

1) Between 1 and 3.7 s, after the first step steer, as F is slightly less than 1, r_{ref} is reduced to a value close to r_s, but higher than r_s [see (2)], and $|\beta|$ stabilizes on values larger than $\beta_{act} = 1.5°$, but smaller than $\beta_{th} = 6°$. This happens also after the second steering application.

2) After the third step steer, when the tire-road friction coefficient decreases from 1 to 0.5, r_s almost halves, which is consistent with the reduction of the lateral acceleration caused by the low tire-road friction coefficient.

3) After the fourth step steer, when the friction coefficient increases from 0.5 to 0.8, the lateral acceleration increases, and therefore, r_s and r_{ref} increase accordingly, thus providing adaptation to the variation of the road conditions.

The performance indicators in Table IV highlight the following.

1) The ISMC provides the best yaw rate tracking performance and for this reason, is selected for the experimental analysis of Section IV.

2) The H$_\infty$ controller provides similar IACA and sideslip peak values with respect to the ISMC, but with worse yaw rate tracking.

3) The performance of the FF + PI is consistently worse than that of the H$_\infty$ and ISMC, because of the destabilizing feedforward contribution designed for high friction conditions. On the other hand, the FF + PI keeps the vehicle in safe conditions with an approximately halved control effort with respect to the other formulations.

4) In the passive and YR-ISMC cases, the peak values of $|\beta|$ and $|\beta_D|$ are coincident, as the maximum sideslip angle values are reached in the final part of the test, when the steering wheel action has already been completed and the kinematic sideslip angle is zero. This situation is typical of uncontrollable vehicle behavior.

In general, the valuable conclusion is that the reference yaw rate formulation has a much greater impact on the results than the selected feedback control structure.

IV. EXPERIMENTAL RESULTS

Experimental tests in dry tarmac conditions (with a tire-road friction coefficient of $\approx$1) were executed at the Kristalpark proving ground (Belgium) with the iCOMPOSE electric vehicle prototype in: 1) the enhanced sport mode that induces high sideslip angles to allow vehicle drift and 2) the passive

Fig. 13. iCOMPOSE electric vehicle demonstrator with the Corrsys Datron sensor mounted at the front end.

TABLE V
PERFORMANCE INDICATORS OF THE CONTROLLED VEHICLE FOR THE
EXPERIMENTAL STEP STEER TESTS (ISMC WITH
$\Delta a_y = 1$ m/s^2 AND $k_1 = k_2 = 1$)

	YR-ISMC	ISMC $\beta_{th} = 6$ deg $\beta_{act} = 1.5$ deg	ISMC $\beta_{th} = 14$ deg $\beta_{act} = 5$ deg	ISMC $\beta_{th} = 20$ deg $\beta_{act} = 10$ deg
RMSE$_r$ (deg/s)	3.69	3.62	3.13	3.13
RMSE$_\beta$ (deg/s)	0	6.39	4.94	3.85
IACA (Nm)	1911	1999	1357	1233
max$|\beta|$ (deg)	29.79	6.89	13.74	20.09
max$|\beta_D|$ (deg)	32.77	9.92	16.74	23.10

Fig. 14. Experimental results, enhanced sport mode, and passive vehicle, step steer, 80 km/h, 100° of final steering wheel angle, YR-ISMC, and ISMC ($\Delta a_y = 1$ m/s^2 and $k_1 = k_2 = 1$). (a) Sideslip angle for the controlled vehicle for different values of β_{th} and for the passive vehicle. (b) Yaw rates for $\beta_{th} = 20°$. (c) Total left- and right-hand sides wheel torque levels for different values of β_{th}.

vehicle configuration, with equal wheel torque values on the four corners. The controller was implemented on the dSPACE AutoBox system installed on the demonstrator. The vehicle features four electric drivetrains, each comprising a switched reluctance on-board motor, which is connected to the wheels through a single-speed transmission system, constant velocity joints, and a half-shaft. A Corrsys Datron S-350 sensor was used to measure the sideslip angle (Fig. 13). Right-hand 100° step steering inputs were applied at a rate of approximately 400°/s, from an initial speed of 80 km/h, in conditions of constant torque demand. The maneuvers were performed with the following controller configurations: 1) YR-ISMC; 2) ISMC with $\beta_{th} = 6°$ and $\beta_{act} = 1.5°$; 3) ISMC with $\beta_{th} = 14°$ and $\beta_{act} = 5°$; and 4) ISMC with $\beta_{th} = 20°$ and $\beta_{act} = 10°$.

Fig. 14(a) shows the measured sideslip angle for the different configurations; Fig. 14(b) plots r_s, r_h, r_{ref}, and r for $\beta_{th} = 20°$; Fig. 14(c) includes the total wheel torque demands on the left- and right-hand sides of the vehicle for different control settings. Table V reports the respective performance indicators. The YR-ISMC leads to a divergent β behavior; instead, with the sideslip-based reference yaw rate correction, β converges to a steady-state value that is consistent with β_{act} and β_{th}, confirming the effectiveness of the proposed scheme. In particular, in Fig. 14(b), r_{ref} is initially equal to r_h, then at ≈ 2 s, the sideslip-based correction is activated as $|\beta| > \beta_{act}$ [see Fig. 14(a)], and the magnitude of r_{ref} decreases, reaching r_s at ≈ 3.5 s. In Table V, RMSE$_\beta$ decreases with β_{th}, which means that for low sideslip thresholds the controller applies a greater yaw rate correction to limit the sideslip angle. On the other hand, RMSE$_r$ does not significantly change among the four controlled configurations, because the same high-level controller, i.e., the PI with the integral sliding mode perturbation compensator, is adopted.
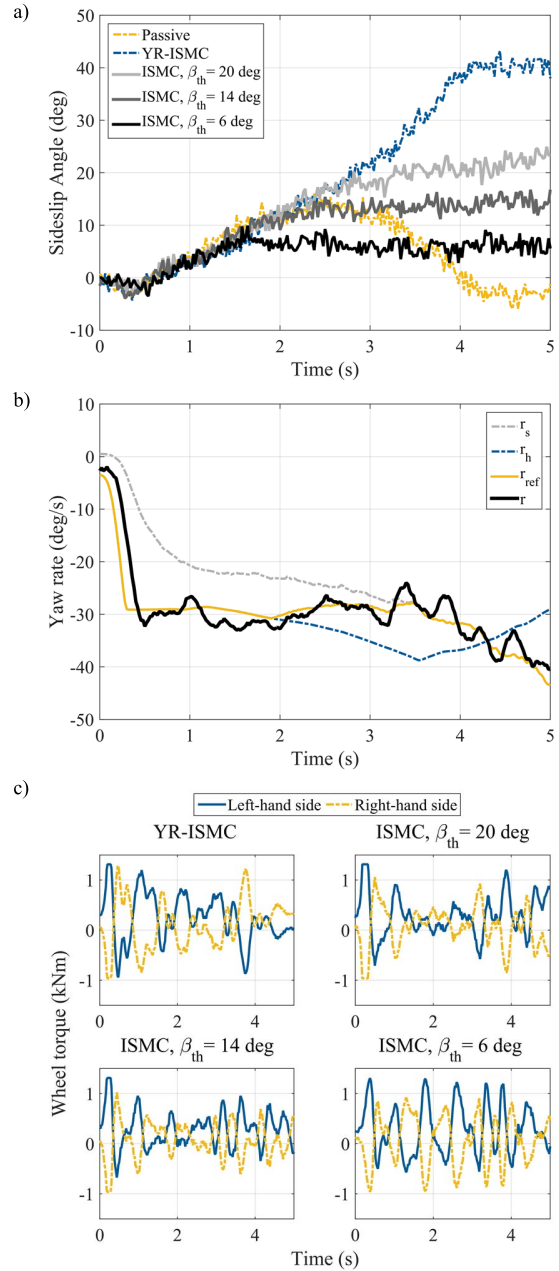
An experimental sensitivity analysis was carried out to understand the effect of the tuning parameters β_{act} [see Fig. 15(a)] and Δa_y [see Fig. 15(b)] during the same maneuver. In particular, in Fig. 15(a), if β_{act} is too small, the sideslip-based correction intervenes too early, causing β to differ from that of the YR-ISMC case much earlier than β_{th}; in particular, from $t = 1.5$–2 s, β increases slowly and reaches β_{th} only at a later stage of the maneuver, hindering the purpose of the enhanced sport mode. In contrast, if β_{act} is too large, the sideslip-based correction intervenes too late, causing significant overshoots of β with respect to β_{th}. In Fig. 15(b),
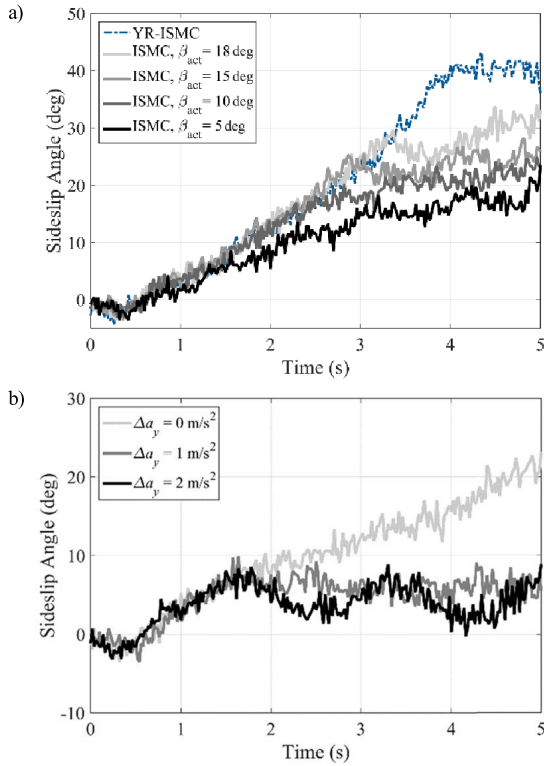
Fig. 15. Experimental results, enhanced sport mode, step steer, 80 km/h, 100° of final steering wheel angle, YR-ISMC, and ISMC ($k_1 = k_2 = 1$). (a) Sideslip angle for different values of β_{act}, with $\beta_{th} = 20°$ and $\Delta a_y = 1$ m/s². (b) Sideslip angle for different values of Δa_y, with $\beta_{act} = 1.5°$ and $\beta_{th} = 6°$.

$\Delta a_y = 0$ m/s² does not guarantee a sufficient sideslip-based correction, while $\Delta a_y = 2$ m/s² causes oscillations of β around β_{th}.

Overall, the experimental sensitivity analysis highlights the importance of appropriate tuning of the controller parameters and the general predictability of the system response depending on the controller setup. This makes the proposed reference yaw rate formulation suitable for vehicle testing engineers without prior knowledge in advanced control theory, and will facilitate its industrial implementation.

V. Conclusion

The analysis of this article leads to the following conclusions.

1) Effective continuously active control of yaw rate and sideslip angle is accomplishable with a SISO formulation—a feedback yaw rate controller in which the reference yaw rate is modified according to the actual sideslip angle. In particular, if the vehicle operates at the limits of handling and the sideslip angle exceeds a tunable threshold, the reference yaw rate approaches the so-called stability yaw rate (which is a function of the measured lateral acceleration) and the yaw rate controller operates as a sideslip rate regulator.

2) The controlled system with the proposed SISO formulation was modeled as a switched linear system, and the related theory was used to infer controller stability.

Frequency domain analyses were adopted to systematically understand the effect of the controller parameters on the system response.

3) The proposed SISO controller significantly increases the stable region of vehicle operation on the $\dot{\beta}(t)$-$\beta(t)$ phase–plane, both in the sport mode and the enhanced sport mode. A new equilibrium appears for initial conditions that are unstable with the feedback controller only based on yaw rate. The new equilibrium is determined by the thresholds of the sideslip-based yaw rate correction.

4) The simulations show that the continuous actuation of direct yaw moment control based on yaw rate tracking without adaptability to swiftly variable tire-road friction conditions can generate more safety-critical vehicle response than a vehicle with constant wheel torque distribution. In contrast, the proposed sideslip-based reference yaw rate correction provides safe vehicle operation in the same conditions and limits the yaw rate overshoots by providing intrinsic tire-road friction adaptation with a simple control structure.

5) Several feedback controllers were assessed with the sideslip-based reference yaw rate correction. In particular, the ISMC formulation provides better performance than the FF + PI and H_∞ controllers. However, the reference yaw rate formulation has higher impact on the results than the selected feedback control structure.

6) The experimental tests demonstrated the operation of the proposed yaw rate formulation in controlled drift conditions with multiple sideslip angle thresholds, and the easy and predictable tunability of the sideslip angle limitation.

References

[1] E. Esmailzadeh, A. Goodarzi, and G. R. Vossoughi, "Optimal yaw moment control law for improved vehicle handling," *Mechatronics*, vol. 13, no. 7, pp. 659–675, 2003.

[2] M. Canale, L. Fagiano, A. Ferrara, and C. Vecchio, "Comparing internal model control and sliding-mode approaches for vehicle yaw control," *IEEE Trans. Intell. Transp. Syst.*, vol. 10, no. 1, pp. 31–41, Mar. 2009.

[3] K. Sawase, Y. Ushiroda, and T. Miura, "Left-right torque vectoring technology as the core of super all wheel control (S-AWC)," *Mitsubishi Motors Tech. Rev.*, vol. 18, pp. 16–23, Apr. 2006.

[4] Z. Wang, U. Montanaro, S. Fallah, A. Sorniotti, and B. Lenzo, "A gain scheduled robust linear quadratic regulator for vehicle direct yaw moment control," *Mechatronics*, vol. 51, pp. 31–45, May 2018.

[5] E. Siampis, E. Velenis, S. Gariuolo, and S. Longo, "A real-time nonlinear model predictive control strategy for stabilization of an electric vehicle at the limits of handling," *IEEE Trans. Control Syst. Technol.*, vol. 26, no. 6, pp. 1982–1994, Nov. 2018.

[6] R. Wang, H. Zhang, and J. Wang, "Linear parameter-varying controller design for four-wheel independently actuated electric ground vehicles with active steering systems," *IEEE Trans. Control Syst. Technol.*, vol. 22, no. 4, pp. 1281–1296, Jul. 2014.

[7] M. Jalali, A. Khajepour, S.-K. Chen, and B. Litkouhi, "Integrated stability and traction control for electric vehicles using model predictive control," *Control Eng. Pract.*, vol. 54, pp. 256–266, Sep. 2016.

[8] L. De Novellis, A. Sorniotti, and P. Gruber, "Driving modes for designing the cornering response of fully electric vehicles with multiple motors," *Mech. Syst. Signal Process.*, vols. 64–65, pp. 1–15, Dec. 2015.

[9] L. De Novellis, A. Sorniotti, P. Gruber, and A. Pennycott, "Comparison of feedback control techniques for torque-vectoring control of fully electric vehicles," *IEEE Trans. Veh. Technol.*, vol. 63, no. 8, pp. 3612–3623, Oct. 2014.

[10] B. Lenzo, A. Sorniotti, G. De Filippis, P. Gruber, and K. Sannen, "Understeer characteristics for energy-efficient fully electric vehicles with multiple motors," in *Proc. World Electr. Vehicle Symp. (EVS)*, Montreal, QC, Canada, 2016, pp. 1–10.

[11] A. Pennycott, L. De Novellis, P. Gruber, A. Sorniotti, and T. Goggia, "Enhancing the energy efficiency of fully electric vehicles via the minimization of motor power losses," in *Proc. IEEE Int. Conf. Syst., Man, Cybern. (SMC)*, Oct. 2013, pp. 4167–4172.

[12] H. Fujimoto and S. Harada, "Model-based range extension control system for electric vehicles with front and rear driving–braking force distributions," *IEEE Trans. Ind. Electron.*, vol. 62, no. 5, pp. 3245–3254, May 2015.

[13] B. Lenzo *et al.*, "Torque distribution strategies for energy-efficient electric vehicles with multiple drivetrains," *ASME J. Dyn. Syst., Meas. Control*, vol. 139, no. 12, 2017, Art. no. 121004.

[14] G. De Filippis, B. Lenzo, A. Sorniotti, P. Gruber, and W. De Nijs, "Energy-efficient torque-vectoring control of electric vehicles with multiple drivetrains," *IEEE Trans. Veh. Technol.*, vol. 67, no. 6, pp. 4702–4715, Jun. 2018.

[15] R. Wang and J. Wang, "Tire-road friction coefficient and tire cornering stiffness estimation based on longitudinal tire force difference generation," *Control Eng. Pract.*, vol. 21, no. 1, pp. 65–75, 2013.

[16] Z. Qi, S. Taheri, B. Wang, and H. Yu, "Estimation of the tyre–road maximum friction coefficient and slip slope based on a novel tyre model," *Vehicle Syst. Dyn.*, vol. 53, no. 4, pp. 506–525, 2015.

[17] C. Voser, R. Y. Hindiyeh, and J. C. Gerdes, "Analysis and control of high sideslip manoeuvres," *Vehicle Syst. Dyn.*, vol. 48, pp. 317–336, Nov. 2010.

[18] B. Lenzo, A. Sorniotti, P. Gruber, and K. Sannen, "On the experimental analysis of single input single output control of yaw rate and sideslip angle," *Int. J. Automot. Technol.*, vol. 18, no. 5, pp. 799–811, 2017.

[19] G. Baffet, A. Charara, and J. Stephant, "Sideslip angle, lateral tire force and road friction estimation in simulations and experiments," in *Proc. IEEE Int. Conf. Control Appl.*, Oct. 2006, pp. 903–908.

[20] M. Doumiati, A. C. Victorino, A. Charara, and D. Lechner, "Onboard real-time estimation of vehicle lateral tire–road forces and sideslip angle," *IEEE/ASME Trans. Mechatronics*, vol. 16, no. 4, pp. 601–614, Aug. 2011.

[21] Y.-H. J. Hsu, S. M. Laws, and J. C. Gerdes, "Estimation of tire slip angle and friction limits using steering torque," *IEEE Trans. Control Syst. Technol.*, vol. 18, no. 4, pp. 896–907, Jul. 2010.

[22] R. Rajamani, G. Phanomchoeng, D. Piyabongkarn, and J. Y. Lew, "Algorithms for real-time estimation of individual wheel tire-road friction coefficients," *IEEE/ASME Trans. Mechatronics*, vol. 17, no. 6, pp. 1183–1195, Dec. 2012.

[23] D. Chindamo, B. Lenzo, and M. Gadola, "On the vehicle sideslip angle estimation: A literature review of methods, models, and innovations," *Appl. Sci.*, vol. 8, no. 3, p. 355, 2018.

[24] G. Kaiser, "Torque vectoring—Linear parameter-varying control for an electric vehicle," Ph.D. dissertation, Inst. Regelungstechnik E-14, Hamburg Univ. Technol., Hamburg, Germany, 2014.

[25] Q. Lu *et al.*, "Enhancing vehicle cornering limit through sideslip and yaw rate control," *Mech. Syst. Signal Process.*, vol. 75, pp. 455–472, Jun. 2016.

[26] R. Tchamna and I. Youn, "Yaw rate and side-slip control considering vehicle longitudinal dynamics," *Int. J. Automot. Technol.*, vol. 14, no. 1, pp. 53–60, 2013.

[27] M. Shino and M. Nagai, "Yaw-moment control of electric vehicle for improving handling and stability," *JSAE Rev.*, vol. 22, no. 4, pp. 473–480, 2001.

[28] W. J. Manning and D. A. Crolla, "A review of yaw rate and sideslip controllers for passenger vehicles," *Trans. Inst. Meas. Control*, vol. 29, no. 2, pp. 117–135, 2007.

[29] M. Jalali, E. Hashemi, A. Khajepour, S.-K. Chen, and B. Litkouhi, "Integrated model predictive control and velocity estimation of electric vehicles," *Mechatronics*, vol. 46, pp. 84–100, Oct. 2017.

[30] J. Deur, P. Barber, and M. Hancock, "Design of a cascade structure of sideslip and yaw rate control," in *Proc. Int. Symp. Dyn. Vehicles Roads Tracks (IAVSD)*, 2011, pp. 1–2.

[31] R. P. Osborn and T. Shim, "Independent control of all-wheel-drive torque distribution," *Vehicle Syst. Dyn.*, vol. 44, no. 7, pp. 529–546, 2006.

[32] B. Li, A. Goodarzi, A. Khajepour, S.-K. Chen, and B. Litkouhi, "An optimal torque distribution control strategy for four-independent wheel drive electric vehicles," *Vehicle Syst. Dyn.*, vol. 53, no. 8, pp. 1172–1189, 2015.

[33] A. T. van Zanten, "Bosch ESP systems: 5 years of experience," SAE Tech. Paper 2000-01-1633, 2000.

[34] L. De Novellis *et al.*, "Direct yaw moment control actuated through electric drivetrains and friction brakes: Theoretical design and experimental assessment," *Mechatronics*, vol. 26, pp. 1–15, Mar. 2015.

[35] G. W. Teng, L. Xiong, B. Leng, and S. L. Hu, "A novel reference model for vehicle dynamics control," in *Proc. 24th Int. Symp. Dyn. Vehicles Roads Tracks (IAVSD)*, 2015, pp. 1–8.

[36] G. Genta, *Motor Vehicle Dynamics: Modeling and Simulation*. Singapore: World Scientific, 1997.

[37] W. F. Milliken and D. L. Milliken, *Race Car Vehicle Dynamics*. Warrendale, PA, USA: SAE, 1995.

[38] *Integrated Control of Multiple-Motor and Multiple-Storage Fully Electric Vehicles (iCOMPOSE)*. Accessed: Apr. 20, 2018. [Online]. Available: https://www.i-compose.eu/iCOMPOSE

[39] Accessed: Feb. 18, 2018. [Online]. Available: https://ipg-automotive.com/products-services/simulation-software/carmaker/

[40] H. B. Pacejka, *Tyre and Vehicle Dynamics*. Oxford, U.K.: Butterworth-Heinemann, 2006.

[41] Q. Lu, A. Sorniotti, P. Gruber, J. Theunissen, and J. De Smet, "H$_\infty$ loop shaping for the torque-vectoring control of electric vehicles: Theoretical design and experimental assessment," *Mechatronics*, vol. 35, pp. 32–43, May 2016.

[42] Maple, *Maplesoft, a Division of Waterloo Maple*, Waterloo, ON, Canada, 2017.

[43] H. Lin and P. J. Antsaklis, "Stability and stabilizability of switched linear systems: A survey of recent results," *IEEE Trans. Autom. Control*, vol. 54, no. 2, pp. 308–322, Feb. 2009.

[44] J. Löfberg, "YALMIP: A toolbox for modeling and optimization in MATLAB," in *Proc. CACSD Conf.*, Sep. 2004, pp. 284–289.

[45] J. F. Sturm, "Using SeDuMi 1.02, a MATLAB toolbox for optimization over symmetric cones," *Optim. Methods Softw.*, vol. 11, nos. 1–4, pp. 625–653, 1999.

[46] T. Goggia *et al.*, "Integral sliding mode for the torque-vectoring control of fully electric vehicles: Theoretical design and experimental assessment," *IEEE Trans. Veh. Technol.*, vol. 64, no. 5, pp. 1701–1715, May 2015.

[47] A. Tota *et al.*, "On the experimental analysis of integral sliding modes for yaw rate and sideslip control of an electric vehicle with multiple motors," *Int. J. Automot. Technol.*, vol. 19, no. 5, pp. 811–823, 2018.

[48] V. Utkin, J. Guldner, and J. Shi, *Sliding Mode Control in Electro-Mechanical Systems*. New York, NY, USA: Taylor & Francis, 1999.

[49] D. McFarlane and K. Glover, "A loop-shaping design procedure using H$_\infty$ synthesis," *IEEE Trans. Autom. Control*, vol. 37, no. 6, pp. 759–769, Jun. 1992.

[50] R. A. Hyde and K. Glover, "The application of scheduled H$_\infty$ controllers to a VSTOL aircraft," *IEEE Trans. Autom. Control*, vol. 38, no. 7, pp. 1021–1039, Jul. 1993.

[51] D. J. Stilwell and W. J. Rugh, "Interpolation of observer state feedback controllers for gain scheduling," *IEEE Trans. Autom. Control*, vol. 44, no. 6, pp. 1225–1229, Jun. 1999.

[52] F. Farroni, M. Russo, R. Russo, M. Terzo, and F. Timpone, "A combined use of phase plane and handling diagram method to study the influence of tyre and vehicle characteristics on stability," *Vehicle Syst. Dyn.*, vol. 51, no. 8, pp. 1265–1285, 2013.

Basilio Lenzo (M'13) received the M.Sc. degree in mechanical engineering from the University of Pisa, Pisa, Italy, and Scuola Superiore Sant'Anna, Pisa, in 2010, and the Ph.D. degree in robotics from Scuola Superiore Sant'Anna, in 2013.

In 2015 and 2016, he was a Research Fellow with the University of Surrey, Guildford, U.K. He is currently a Senior Lecturer of automotive engineering with Sheffield Hallam University, Sheffield, U.K. His research interests include vehicle dynamics, simulation, control, and robotics.

Mattia Zanchetta received the B.Sc. degree in electronic engineering and telecommunications and the M.Sc. degree in control engineering from the University of Pavia, Pavia, Italy, in 2013 and 2016, respectively.

He is currently a Ph.D. Researcher with the University of Surrey, Guildford, U.K. His research interests include vehicle dynamics and control and autonomous driving.

Patrick Gruber received the M.Sc. degree in motorsport engineering and management from Cranfield University, Cranfield, U.K., in 2005, and the Ph.D. degree in mechanical engineering from the University of Surrey, Guildford, U.K., in 2009.

He is currently a Reader of advanced vehicle systems engineering with the University of Surrey. His research interests include vehicle dynamics and tire dynamics with special focus on friction behavior.

Aldo Sorniotti (M'12) received the M.Sc. degree in mechanical engineering and the Ph.D. degree in applied mechanics from the Politecnico di Torino, Turin, Italy, in 2001 and 2005, respectively.

He is currently a Professor of advanced vehicle engineering with the University of Surrey, Guildford, U.K., where he coordinates the Centre for Automotive Engineering. His research interests include vehicle dynamics control and transmission systems for electric and hybrid electric vehicles.

Wouter De Nijs received the M.Sc. degree in mechanical engineering in the field of mechatronics from KU Leuven, Leuven, Belgium, in 2006.

He is currently a Core Lab Manager with Flanders Make, a Flemish Strategic Research Centre for the Manufacturing Industry, Leuven. His lab performs precompetitive industry driven research on novel sensing, monitoring, control, and decision-making solutions in the application fields of vehicles-, machines-, and factories-of-the-future.